Available online at www.sciencedirect.com
ScienceDirect
Ceramics International 35 (2009) 3313–3320
CERAMICS INTERNATIONAL
www.elsevier.com/locate/ceramint

Phase formation during liquid phase sintering of ZnO ceramics

Mohammad Lutful Arefin [a,*], Friedrich Raether [a], David Dolejš [b,c], Andreas Klimera [a]

[a] Fraunhofer-Institut Silicatforschung (ISC), Neunerplatz 2, 97082 Würzburg, Germany
[b] Bayerisches Geoinstitut, University of Bayreuth, 95440 Bayreuth, Germany
[c] Institute of Petrology and Structural Geology, Charles University, 12843 Praha 2, Czech Republic

Received 20 February 2009; received in revised form 6 March 2009; accepted 23 May 2009
Available online 18 June 2009

Abstract

ZnO doped with Bi_2O_3 and Sb_2O_3 (ZBS), is the basic system for ceramic varistors. Phase formation during sintering of ZBS was measured in situ, using 1 mm thick samples and synchrotron X-rays. Sintering shrinkage was measured in different atmospheres by an optical method. Thermodynamic calculations were performed to explain phase formation, composition, stability of additive oxides and influence of the oxygen fugacity on sintering. Sb_2O_4, pyrochlore, trirutile and spinel were formed at temperatures of 500–800 °C. The oxidation of antimony was controlled by the oxygen partial pressure and affected both, phase formation and sintering kinetics, in the ZBS system.

Keywords: E. Varistors; Liquid phase sintering; Electroceramics; High temperature X-ray diffraction; Thermodynamic simulation; Oxygen fugacity

1. Introduction

The highly non-linear electrical properties of the ZnO ceramics have made it an indispensable material for varistor industries. It was studied since the early seventies [1]. The exceptional current–voltage behaviour of ZnO varistors was attributed mainly to the presence of the Bi_2O_3 additive. In addition, Bi_2O_3 strongly alters the sintering behaviour of ZnO. It produces a liquid phase with ZnO by eutectic melting at 738 °C [2] and enables liquid phase sintering. During cooling, it forms tunnel barriers at the ZnO grain boundaries and this leads to the non-ohmic behaviour [3]. Besides Bi_2O_3, Sb_2O_3 is used as a major additive in ZnO varistor ceramics, leading to the ZBS ($ZnO + Bi_2O_3 + Sb_2O_3$) system. Apart from the melt phase, many other phases exist during sintering of the ZBS system, known from early works by Wong and Inada [4–6]. In these studies phases were identified by X-ray diffraction (XRD) at ambient temperature. All three ZBS components form a pyrochlore phase which has the nominal stoichiometry $Zn_2Bi_3Sb_3O_{14}$ [4]. Miles and West showed that two different pyrochlore phases with slightly different stoichiometry coexist in the ZBS system at ambient temperature [7]. ZnO and Sb_2O_3 form a trirutile phase with the stoichiometry $ZnSb_2O_6$ [8] and spinel phases. The spinel phases have a cubic ($Zn_{2.33}Sb_{0.67}O_4$) and orthorhombic ($Zn_7Sb_2O_{12}$) structure [5,9]. Leite et al. [10] studied the microstructural evolution in the ZBS system with high temperature X-ray diffractometry (HT-XRD). They identified trirutile, pyrochlore and spinel and suggested the following reaction sequence:

At 527 °C,

$$Sb_2O_3(s) + O_2 \rightarrow Sb_2O_5(l) \quad (1)$$

At 700–800 °C,

$$Sb_2O_5(l) + ZnO(s) \rightarrow ZnSb_2O_6(s) \quad (2)$$

At >800 °C,

$$ZnSb_2O_6(s) + 6ZnO(s) \rightarrow Zn_7Sb_2O_{12}(s) \quad (3)$$

Between 700 °C and 900 °C,

$$3ZnSb_2O_6(s) + 3Bi_2O_3(s) + ZnO(s) \rightarrow 2Zn_2BI_3Sb_3O_{14}(s) \quad (4)$$

The pyrochlore phase is formed at temperatures between 700 °C and 900 °C (see Eq. (4) above). It had an impact on densification kinetics [10]. The spinel phase inhibits grain growth of the ZnO grains and retards densification [8].

* Corresponding author. Tel.: +49 0 931 4100 248; fax: +49 0 931 4100 299.
E-mail address: arefin@isc.fraunhofer.de (M.L. Arefin).

0272-8842/$36.00
doi:10.1016/j.ceramint.2009.05.030

Antimony changes its valency from Sb^{3+} to Sb^{5+} when spinel and pyrochlore are formed from Sb_2O_3 meaning that additional oxygen is required from the atmosphere. This can create gradients from the surface to the interior of the compacts during heat treatment when oxygen access is limited by diffusion through the pore channels. In production furnaces, oxygen access may be further limited by the large packing density of ZnO green parts. The burn off of binder components during binder removal also can create oxygen deficient atmospheres. Antimony and bismuth oxides have a large vapour pressure which lead to some evaporation during sintering – especially at high temperatures [4,11]. This evaporation can produce additional gradients in the components with higher concentration of volatile species in the interior of the parts. Evaporation rate depends on the partial pressure of evolved components in the furnace atmosphere which is controlled by gas flow and packing density of the parts.

Few in situ investigations were done by HT-XRD [10,12]. But in these studies Cu Kα X-rays were used which have a penetration depth as small as 15 μm in ZnO ceramics [13]. Due to gas phase reactions discussed in the previous paragraph, it was expected that the phase formation at the surface of ZBS samples can differ significantly from the phase formation in the bulk material. In the present paper phase formation in the ZBS system was studied in situ by HT-XRD, using synchrotron X-rays. This enables the analysis of bulk samples and avoids surface effects. Additionally, sintering kinetics of ZBS green samples were measured by optical dilatometry. The optical measurements enabled dilatometric studies in closed crucibles, where the concentration of evolved species could be systematically varied. The investigation was complemented by thermodynamic modelling and thermal analysis to get a better understanding of atmosphere effects on sintering of varistor ceramics.

2. Experimental techniques

2.1. Sample preparation

Green samples were prepared after dry milling ZnO, Sb_2O_3 and Bi_2O_3 powders (ABB, Switzerland) separately in a tungsten carbide vibrating cup mill (Fritsch Pulverisette 9, Fritsch, Idar-Oberstein, Germany) for 3 min each. The particle size ($D_{0.5}$) after milling was determined in iso-propanol, using laser light scattering (Mastersizer S, Malvern Instruments GmbH, Herrenberg, Germany). The data are shown in Table 1.

The isoelectric points of the powders were measured by electrokinetic sonic amplitude (ESA, AcoustoSizer II, Agilent Technologies, Inc., Santa Clara, USA) to be 8.4–9.4, 9.8 and 2.7–3.2 for ZnO, Bi_2O_3 and Sb_2O_3 respectively. The milled powders were mixed with appropriate amounts of ZnO, Bi_2O_3 and Sb_2O_3 and distilled water. The pH value of the slurry was 7.5. Mixing was done in a planetary ball mixer for 24 h. A zirconia container and zirconia balls were used to avoid any impurity from the lining. The mixture was dried for 12 h at 130 °C and pushed through a sieve with 2 mm × 2 mm mesh size. The fragments were filled into silicon moulds and cold isostatically pressed at 100 MPa. Cylindrical compacts were produced with an average diameter of 19 mm and a density of 3.4 g/cm^3 – corresponding to a fractional density of 60%. The respective green samples were cut from the pressed compacts, using a SiC cutting wheel.

Table 1
Particle size ($D_{0.5}$) of raw powders in μm before and after milling.

	ZnO	Sb_2O_3	Bi_2O_3
Raw $D_{0.5}$	1.82	3.29	4.42
Milled $D_{0.5}$	1.56	2.48	3.29

2.2. Thermal analysis

Differential thermal analysis (DTA) was done with NETZSCH STA409 (Netzsch Gerätebau GmbH, Selb, Germany) and thermogravimetry (TG) was conducted using a thermobalance (SETARAM TAG24, Setaram, Caluire Cedex, France). Binary mixtures of the raw powder were prepared with ZnO and Sb_2O_3 and with ZnO and Bi_2O_3 at a molar ratio of 1:1. Small disc shaped samples with 10 mm diameter and 2 mm thickness were formed from these mixtures and heated at 10 K/min up to 1000 °C in atmospheres of O_2-, Ar- and synthetic air, respectively.

2.3. High temperature X-ray diffraction

Since the evaporation of volatile species led to concentration gradients near the surface, HT-XRD using Cu Kα X-rays reflects surface reactions, but not the bulk properties of the varistor ceramics. Therefore, white synchrotron X-rays from a 4.5 GeV bending magnet (E_c = 16 keV) source were used at the HASYLAB, Hamburg. Samples of 1 mm thickness could be analysed in transmission.

Fig. 1 shows the schematic of the experimental setup. The disc shaped samples (diameter 19 mm, thickness 1 mm) were clamped between two sintered ZnO discs with circular holes in the middle, to allow X-rays to pass through. The stack was mounted in a small resistive heated horizontal tube furnace, which was controlled through a programmable thermo-regulator.

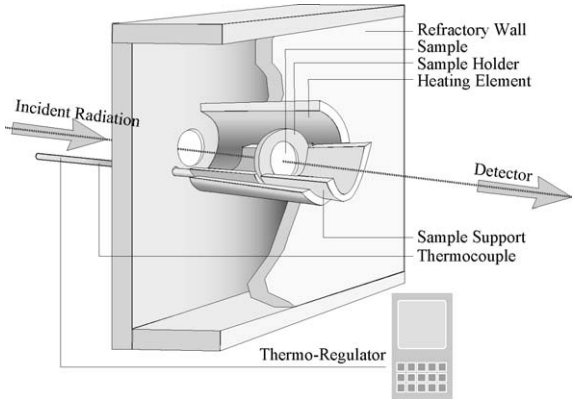

Fig. 1. Sectioned view of the experimental setup used for HT-XRD during sintering of ZnO ceramics at the HASYLAB, Hamburg.

The symmetry axis of the furnace was aligned with the beam axis and the detector.

A Ge-detector, cooled with liquid nitrogen, was used at a fixed angle for energy dispersive measurement of the diffracted X-rays. Energy resolution $\Delta d/d$ was 10^{-2} FWHM (full width at half maximum) above 26 keV. Energy calibration was done with a mixed target of Ge, Mo, Sn, Ba, W and Gd. The total amount of $Sb_2O_3 + Bi_2O_3$ additives in the ZBS samples, used for X-ray diffraction studies, was 6 mol%. This was higher than in the study of sintering shrinkage (see next paragraph) to obtain a better detection of minor phases. Three different Sb_2O_3:Bi_2O_3 molar ratios of 1:1, 1:2 and 2:1 were used. Heating rate was 5 K/min and furnace atmosphere was ambient air. Temperature calibration of the furnace was performed at two temperatures by the melting of Au and NaCl at 1064.18 °C and 801 °C respectively.

The phase evaluations were done by DIFFRAC^{plus} evaluation package (Bruker AXS GmbH, Karlsruhe, Germany) after converting the in-situ data from energy scale (channels) to angular scale (2θ), according to the wavelength of Cu Kα X-rays (0.154 nm). The database of ICSD (Fachinformationszentrum FIZ, Karlsruhe, Germany) was used for phase identification.

2.4. Optical dilatometry

For optical dilatometry, cylinders of 20 mm height and 19 mm diameter were prepared by machining the pressed compacts. For dilatometry, the total amount of $Sb_2O_3 + Bi_2O_3$ additives in the ZBS samples was 1.5 mol% and 6.0 mol% respectively. Fig. 2 shows a sketch of the optical dilatometer (TOMMI, Fraunhofer ISC, Würzburg, Germany). It uses the shadow of the sample which is illuminated by a halogen lamp. The sample contour is detected by special contour tracking algorithm. Dimensional changes of the sample are extracted from the sample contour [8]. A $MoSi_2$ heated chamber furnace, operating in air (flow rate 10 l/min) was used for these measurements.

The ZBS sample was placed in an alumina crucible ($42 \times 30 \times 25$ mm^3) with closed lid to increase the partial pressure of gas species, evolved during the heat treatment. The crucible was equipped with sapphire windows to enable light transmission. To study the effect of atmosphere on sintering kinetics, loose powders of Sb_2O_3 or Bi_2O_3 (approx. 2 g) were used in the crucible. The powders had no contact to the ZBS sample. Shrinkage L/L_0 was measured using the width of the samples scaled by the initial width at the start of the measurement. Correction for thermal expansion was done by a 2nd order polynomial fitted to the expansion curve obtained from sintered ZBS sample in the required temperature range. Onset temperature of sintering was determined from the $L/L_0(T)$ diagram by the intersection of the tangents before shrinkage and at 2% shrinkage. Temperature was measured with a Pt–PtRh thermocouple outside the crucible.

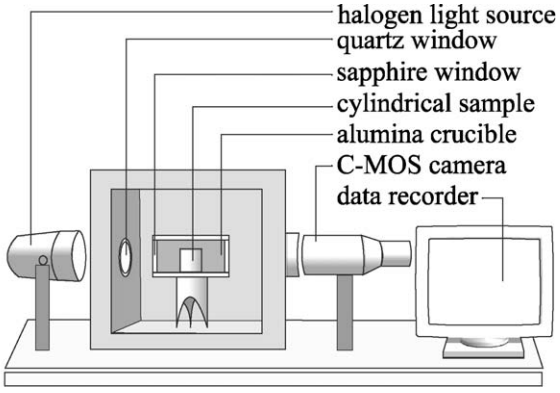

Fig. 2. Schematic diagram of the optical dilatometer and the crucible used for measuring sintering shrinkage.

2.5. Thermodynamic simulations

The aim of thermodynamic modelling was to address melt formation, its compositional range, stability of solid phases and the effect of oxygen fugacity on the progress of sintering. A thermodynamic dataset [11] for solid, liquid and gaseous species in the system Bi–Sb–Zn–O was compiled. Liquid phase in the Bi–O system was described by the two-sub-lattice ionic model [14], whereas the multicomponent oxide liquid was best reproduced by associate model with small symmetric contribution to the enthalpy of mixing (−13 kJ/mol) between ZnO and Bi_2O_3, and ZnO and Sb_2O_3. Gas phase was an ideal mixture of multiple oxide species. Phase equilibrium calculations were performed with the Theriak-Domino code [15].

3. Results

3.1. Thermodynamic simulations

Fig. 3 shows that partial pressure of oxygen, i.e. oxygen fugacity has a significant effect on the stability of antimony oxides. At low temperatures in air, Sb_2O_5 is stable but it

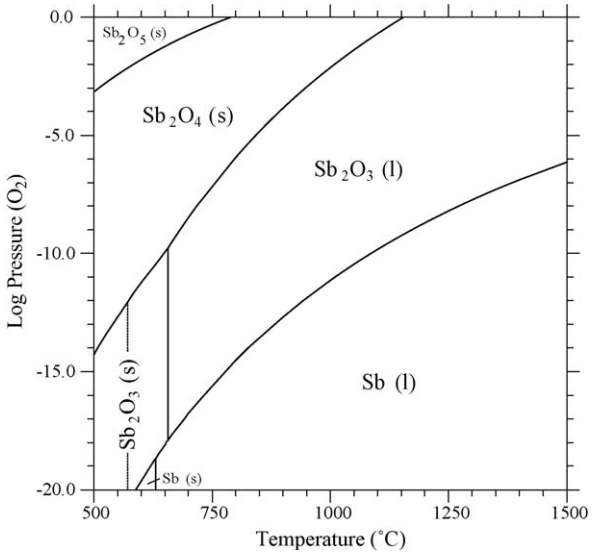

Fig. 3. Equilibrium states in the Sb–O system as a function of temperature and O_2 partial pressure.

becomes progressively reduced to Sb_2O_4 at 780 °C and to Sb_2O_3 at 1150 °C. Sb_2O_4 is predicted to be a stable phase within the range of our experimental temperature and pressure (750–1150 °C, 0.2–1 bar), see also [16]. Therefore, it is assumed that solid Sb_2O_4 forms during initial stages of sintering and it restricts melt productivity due to its refractory character. This is in agreement with our HT-XRD results (see below).

In the Bi–O system, the Bi_2O_3 phase is stable over the whole temperature range (Fig. 4). α-Bi_2O_3 undergoes solid-solid transformation to δ-polymorph at 730 °C and the latter melts at 825 °C. At high temperatures increasing miscibility between Bi_2O_3 (l) and Bi(l) is responsible for variation of melt composition with oxygen partial pressure. At oxygen saturation, the calculated liquid composition remains very close to Bi_2O_3.

During sintering, starting oxides (Bi_2O_3, Sb_2O_3) undergo vaporization which creates undesirable gradients in the composition and porosity near the sample surface. In order to assess the gas composition and factors that can control it, gas speciation and vapour pressures of individual species were calculated (Fig. 5).

In the system Sb–O, the vapour is dominated by Sb_4O_6 species with a vapour pressure of $10^{-1.8}$ bar at 1000 °C (Fig. 5a). Note that vapour pressures are shown in equilibrium to the most stable condensed phase at the respective oxygen partial pressure. Elemental gaseous species (Sb, Sb_2 and Sb_4) have partial pressures less than 10^{-12} bar over molten oxide and are not significant for a selective element removal. It can be seen that the vapour pressure of Sb_4O_6 strongly decreases, when Sb_2O_3 is replaced by Sb_2O_4 at an oxygen partial pressure above 10^{-2} bar (Fig. 5a).

In the system Bi–O, vapour pressures vary over several orders of magnitude and reach 10^{-4} bar at 1000 °C in air or oxygen (Fig. 5b). The predominant gaseous species is Bi_4O_6, followed by Bi_2O_3. Vapour pressure of BiO and Bi_3O_4 are two orders of magnitude lower. The results demonstrate that Bi_2O_3 vaporizes congruently, but less efficiently than Sb_2O_3. Reduced gaseous species of bismuth become only stable at extremely reducing conditions, where the vapour pressures increase significantly.

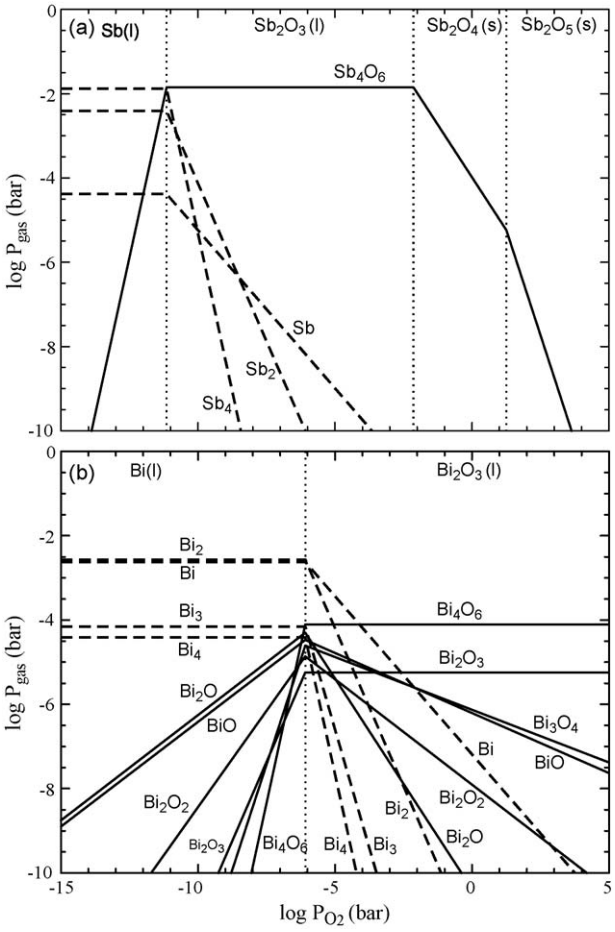

Fig. 5. Vapour pressure over (a) Sb_2O_3- and (b) Bi_2O_3 liquid shown as a function of O_2 partial pressure at 1000 °C.

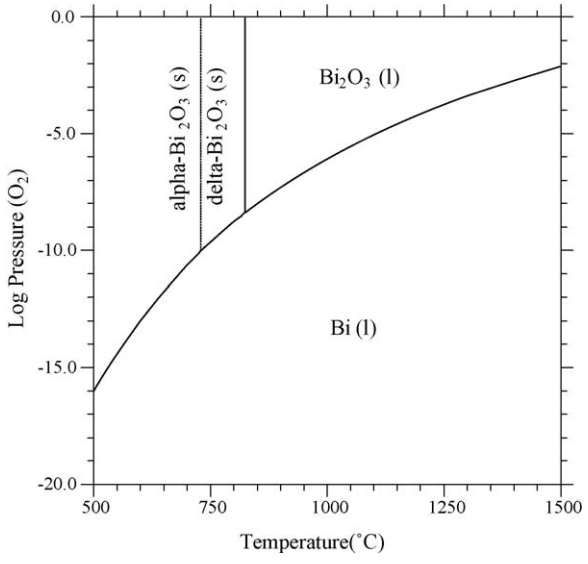

Fig. 4. Equilibrium states in the Bi–O system as a function of temperature and O_2 partial pressure.

Melt formation during sintering was modelled in the Zn–Bi–O and Zn–Bi–Sb–O systems. Fig. 6 shows pseudobinary temperature-composition sections. The system Bi_2O_3–ZnO is characterised by a strongly asymmetric location of the binary eutectic at 750 °C and 89 mol.% Bi_2O_3. The initial melt dissolves minor quantities of zinc oxide only, therefore the amount of melt in the system is controlled by the initial Bi_2O_3 proportion in the sample. The addition of Sb_2O_3 to the system leads to depression of the solidus from 750 °C to 590 °C (Fig. 6b), due to the comparably low melting temperature of Sb_2O_3. As in the previous case, the low temperature melt is dominated by $(Bi, Sb)_2O_3$ and it contains less than 10 mol.% dissolved ZnO. Fig. 6c shows the melt formation in the ternary system Bi_2O_3–Sb_2O_4–ZnO, which corresponds to more oxidizing conditions than the system with Sb_2O_3. Sb_2O_4 is a refractory oxide and the onset of melting changes accordingly. The system is pseudo-ternary and the eutectic melting is not depressed below 760 °C. At these conditions, four phases are present: $(Bi, Sb)_2O_3$ liquid and Sb_2O_4, Sb_2O_5 and ZnO solid

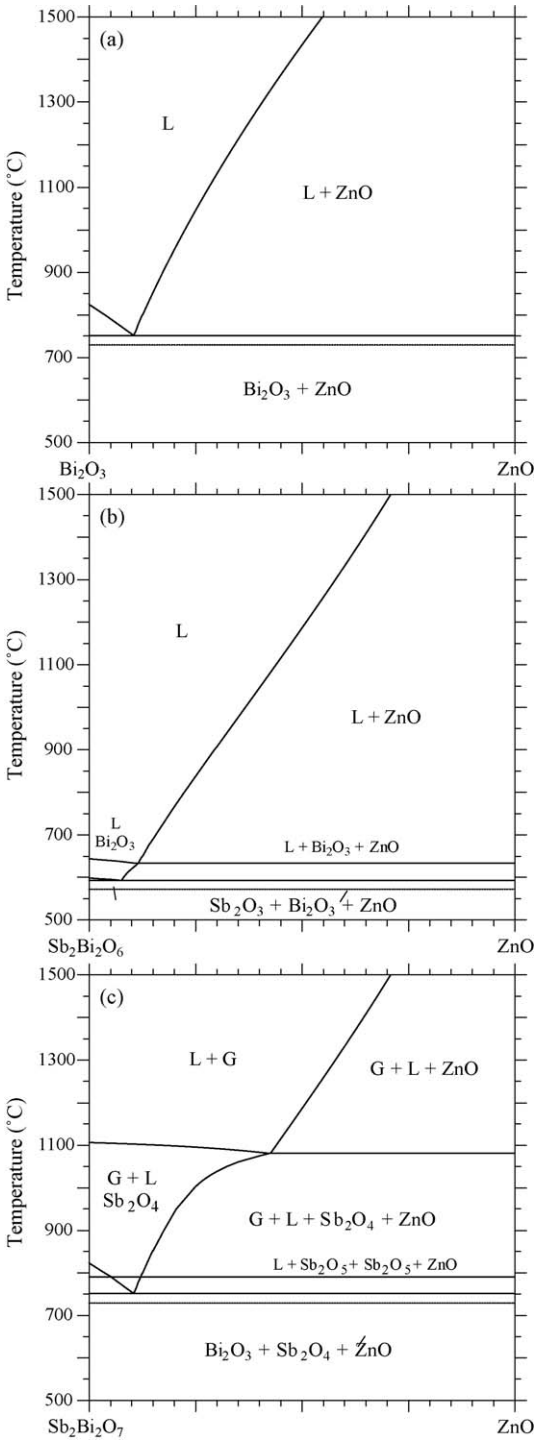

Fig. 6. Calculated temperature-composition sections for (a) ZnO–Bi_2O_3, (b) ZnO–Bi_2O_3–Sb_2O_3 and (c) ZnO–Bi_2O_3–Sb_2O_4 (L = liquid, G = gas).

phases. At 790 °C, Sb_2O_5 disappears and the liquid is saturated with ZnO and Sb_2O_4.

3.2. Thermal analysis

The binary system ZnO–Sb_2O_3 (molar ratio 1:1) showed a weight gain of 4.6% during heating in pure oxygen atmosphere between 510 °C and 550 °C (Fig. 7). This weight gain was

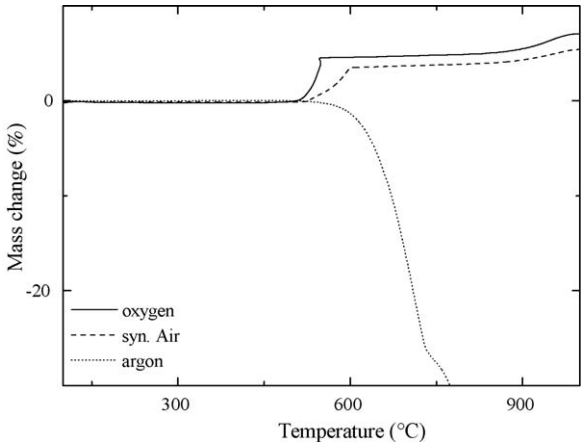

Fig. 7. Mass change as function of temperature of ZnO–Sb_2O_3 sample while heated at 10 K/min up to 1000 °C.

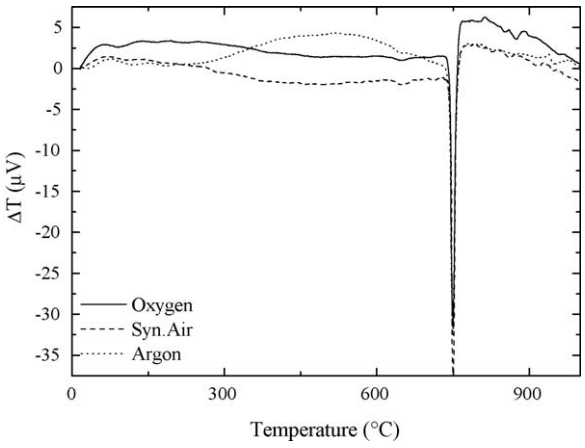

Fig. 8. DTA curves of ZnO–Bi_2O_3 sample showing coincidence of the eutectic point at 749 °C regardless of atmosphere.

attributed to the oxidation from Sb_2O_3 to Sb_2O_4 which should result in an increase of 4.3%. In air a similar weight gain of 3.5% was measured between 520 °C and 600 °C. In argon atmosphere a distinct mass loss of 76% was registered between 520 °C and 920 °C. This mass loss corresponds to a complete evaporation of antimony oxide. The bend in the curve (compare

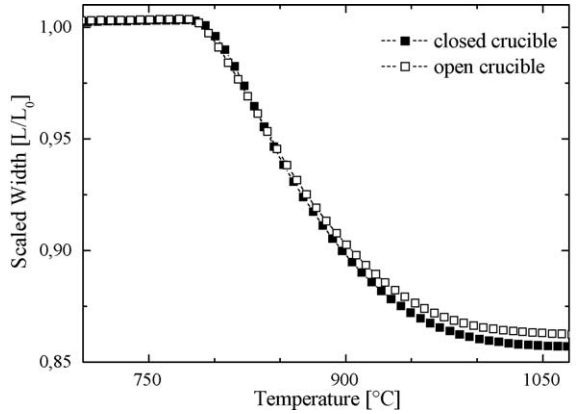

Fig. 9. Shrinkage of ZnO green samples with ratio of Sb_2O_3 to Bi_2O_3 of 1:1 measured with (■) and without (□) a closed crucible.

Table 2
Onset temperatures of shrinkage, densities at 1080 °C and final densities of ZBS samples, sintered in a closed and open crucible respectively.

Samples	Onset temperature (°C)	Density at 1080 °C (from shrinkage data) (g/cm^3)	Final density (by Archimedes) (g/cm^3)
Open	792	93.67	97.86
Closed	798	95.33	98.20

Fig. 7) indicates that reduction of antimony precedes evaporation.

The binary system ZnO–Bi_2O_3 (1:1 molar) showed a weight loss of less than 0.5% regardless of the atmosphere. Fig. 8 shows DTA curves for the binary system ZnO–Bi_2O_3 (molar ratio 1:1) from three different experiments performed with different atmospheres. An endothermic peak at 749 °C was observed for inert and oxidic atmosphere. It was attributed to the eutectic melting of the ZnO–Bi_2O_3 system.

3.3. Optical dilatometry

Fig. 9 shows the shrinkage curves of two ZBS samples with 1.5 mol.% additives (0.75 mol.% Bi_2O_3 and 0.75 mol.% Sb_2O_3), sintered in a closed and an open crucible respectively. Onset temperature was slightly smaller and density was significantly reduced in the open crucible (Table 2).

Fig. 10 shows shrinkage curves for ZBS green samples with 6 mol.% additives (3 mol.% Bi_2O_3 and 3 mol.% Sb_2O_3) sintered in different atmospheres. For the ZBS sample without additional loose powders, shrinkage started at 780 °C. With the addition of loose Sb_2O_3 powder within the alumina crucible, the onset temperature decreased to 762 °C. This was attributed to the oxidation of Sb_2O_3 to Sb_2O_4, which created a reducing atmosphere within the crucible.

It was assumed that the reducing atmosphere led to a lower oxidation state of antimony within the sample and – according to the thermodynamic simulation – to a smaller temperature of melt formation (compare previous section). At higher temperatures, the addition of Sb_2O_3 powder reduced sintering activity (compare Fig. 10). It was assumed that pyrochlore and spinel formation were affected by the reducing atmosphere because additional oxygen was required for the transformation of Sb^{+3} or Sb^{+4} to Sb^{+5}. So the retardation of sintering in the intermediate sintering stage was attributed to a change in the phase formation sequence. The final sintering stage could not be measured with the addition of loose powders, since increasing condensation of volatile species at the sapphire windows of the crucible led to opaque layers at temperatures above 900 °C. With the addition of loose Bi_2O_3 powder, the onset temperature only slightly changed to 790 °C. The decrease of onset temperature from 798 °C to 780 °C when ZBS samples with 1.5, respectively 6 mol.% additives, were sintered in a closed crucible without loose powders (compare Figs. 9 and 10), was attributed to the increasing fraction of melt phase.

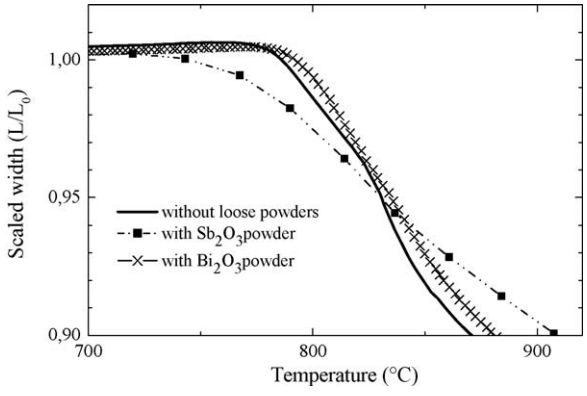

Fig. 10. Effect of Sb_2O_3- and Bi_2O_3 powders addition in closed crucible on the onset of shrinkage in ZBS green samples.

3.4. High temperature X-ray diffraction

Fig. 11 shows the HT-XRD spectra of the ZBS system at a ratio of Sb_2O_3 to Bi_2O_3 of 1:1. Heating rate was 5 K/min. Besides ZnO, different polymorphs of Bi_2O_3 and Sb_2O_3, trirutile, pyrochlore and spinel were identified. From each phase one prominent peak was selected for area determination: ⟨0 4 1⟩ for Bi_2O_3, ⟨4 4 0⟩ for Sb_2O_3, ⟨1 3 4⟩ for γ-Bi_2O_3, ⟨1 1 3⟩ for β-Sb_2O_4, ⟨4 3 3⟩ for $Bi_{38}ZnO_{60}$, ⟨4 4 0⟩ for pyrochlore, ⟨5 1 1⟩ for spinel, ⟨4 8 2⟩ for beta-spinel and ⟨2 1 3⟩ for tri-rutile. Peak area was determined after subtraction of a linear background. The respective peak areas were scaled by the area of the ⟨1 0 2⟩ ZnO peak in the corresponding spectrum. Scaled peak areas are shown in Fig. 12 for the 1:1, 1:2 and 2:1 ratios of Sb_2O_3 to Bi_2O_3. It can be seen that the molar ratio of the additives largely affected phase formation. In all measurements, the primary additives disappeared below 630 °C. Between 500 °C and 800 °C γ-Bi_2O_3 and between 440 °C and 580 °C β-Sb_2O_4 were formed. Note that the

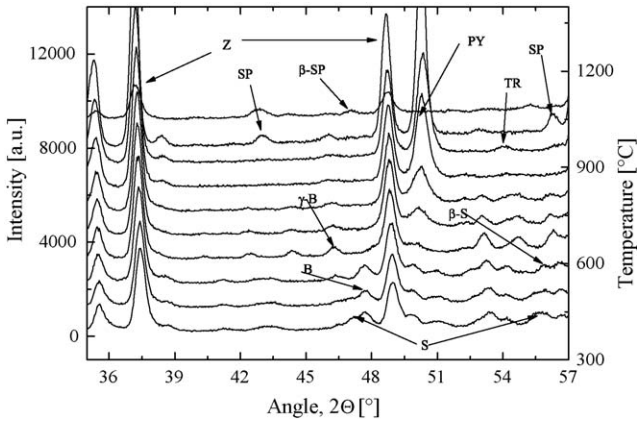

Fig. 11. HT-XRD spectrum showing evolution of phases as functions of temperature. ZnO (Z), Bi_2O_3 (B), γ-Bi_2O_3 (γ-B), Sb_2O_3 (S), β-Sb_2O_4 (β-S), $Bi_{38}ZnO_{60}$ (BZ) and pyrochlore (PY).

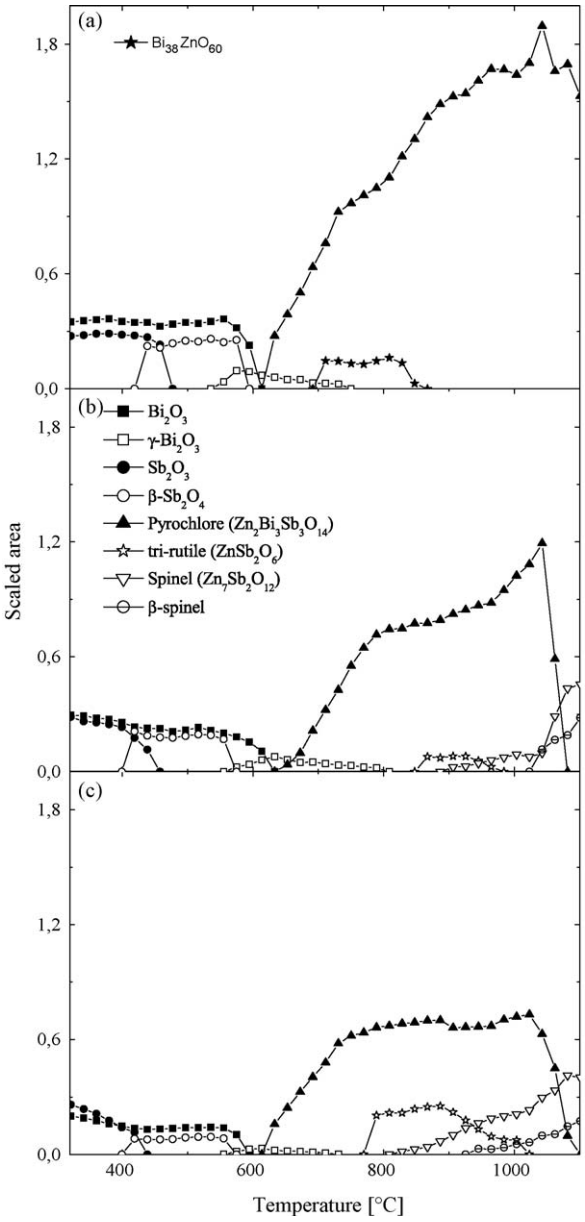

Fig. 12. Scaled peak areas of phases identified during sintering of ZBS samples with the ratio of Sb_2O_3 to Bi_2O_3 of 1:2 (a), 1:1 (b) and 2:1 (c).

temperature of Sb_2O_4 formation is smaller than in the DTA-TG measurement, which was attributed to an inaccurate temperature measurement in the tube furnace used for the HT-XRD measurements in the low temperature regime.

Trirutile was formed between 750 °C and 1000 °C in samples with molar ratios of Sb_2O_3 to Bi_2O_3 of 1:1 and 2:1, but not with 1:2. On the other hand, a binary phase $Bi_{38}ZnO_{60}$ was detected between 650 °C and 860 °C only for the sample with 1:2 ratio (compare Fig. 12a–c). Moreover, no spinel phase was identified for samples with molar ratios of Sb_2O_3 to Bi_2O_3 of 1:2 up to 1100 °C. This was in agreement with findings of Inada [6] for a sample with similar ratio between the two additives.

The pyrochlore phase appeared little above 600 °C and was stable until very high temperature beyond 1000 °C. It increased up to temperatures of 1040 °C and decreased above that temperature. The increase was less pronounced with higher Sb_2O_3 to Bi_2O_3 ratio (compare Fig. 12). With the 1:1 and 2:1 molar ratios, a spinel phase occurred above 850 °C and remained until the end of the process. It was accompanied by a polymorph (β-spinel) at high temperature. The spinel phase showed an increase at 1040 °C when the pyrochlore phase decreased. Trirutile and the spinel phases were detected at lower temperatures in the sample with Sb_2O_3:Bi_2O_3 ratio of 2:1 than in the sample with 1:1 ratio.

4. Discussion

The present HT-XRD and TG measurements show, that the reaction sequence during heating of ZBS samples suggested by Leite (compare Eqs. (1)–(4)) has to be changed. In oxidising atmospheres, Sb_2O_4 is formed from the sequioxide at 530 °C instead of Sb_2O_5. The formation of Sb_2O_4 during the ZBS heat treatment was already reported by Inada [5,6]. Thermodynamic modelling demonstrated that the presence of Sb_2O_4 increases the temperature of melt formation, whereas Sb_2O_3 leads to a decrease of melting temperature. So it was assumed that the oxygen activity in the furnace atmosphere affects the onset temperature of sintering. This was demonstrated in sintering experiments in closed crucibles where the reducing atmosphere was generated by excess Sb_2O_3 powder. A clear decrease of the onset temperature confirmed the thermodynamic model.

Kim et al. have explained the densification characteristics of ZnO doped with Sb_2O_3 by the specific evaporation-condensation behaviour of Sb_2O_3 [17]. Antimony oxides begin to evaporate at approx. 500 °C. They condense on the ZnO particle surfaces as a non-crystalline phase and moderate mass transfer and densification. This mechanism has been confirmed by several independent experimental studies [18,19]. If Sb_2O_3 was oxidized to Sb_2O_4 the vapour pressure is strongly decreased (compare Fig. 5a) and evaporation–condensation is assumed to be retarded. So beside melt formation, a second phenomenon exists which is affected by the oxygen activity in the atmosphere. Although not directly measured, it was concluded from the change in sintering kinetics in the intermediate stage (compare Fig. 10) that oxygen activity also affects the formation of phases where Sb is in the oxidation state +5 (pyrochlore, spinel).

It was argued that Bi which is bound in the pyrochlore phase is not available for melt phase formation [8]. Therefore liquid phase sintering is reduced. Kim et al. had already shown that shrinkage was more affected by the ratio of Sb_2O_3 to Bi_2O_3 than by the absolute concentration of the additives [8]. So, the increase of pyrochlore intensity identified in the HT-XRD measurements at temperatures between 600 °C and 1050 °C is assumed to reduce the melt phase. The decrease of pyrochlore phase measured at higher temperature and the corresponding increase of spinel intensity is believed to increase the melt fraction. This was already proposed by Kim et al. [8].

The thermodynamic analysis in the current work suggests that the trivalent metal oxides Bi and Sb vaporize congruently. By increasing their partial pressure in the environmental atmosphere the vaporization from the sample can be reduced

during sintering. Experiments showed that sintering inside closed crucible considerably improves final densities of ZnO ceramic system compared to open sintering.

5. Conclusions

A number of crystalline phases were identified by HT-XRD during sintering of ZBS green samples: Bi_2O_3, γ-Bi_2O_3, Sb_2O_3, β-Sb_2O_4, trirutile, pyrochlore, spinel and β-spinel. Synchrotron radiation allowed the measurement of bulk properties of the samples due to large penetration depth of the X-rays. Formation of β-Sb_2O_4 was already suggested by thermodynamic simulations and confirmed by DTA measurements as well.

The control of oxygen activity in the furnace atmosphere during sintering of ZBS is required to avoid variations in the oxidation state of antimony. It was shown that sintering kinetics is strongly affected by the presence of Sb_2O_4 and Sb_2O_3 respectively. With increasing partial pressure of oxygen, Sb_2O_4 becomes stable. Its refractory character can help to minimize vapour loss and shift the melt formation to higher temperatures.

Acknowledgements

The authors are grateful to Mr. Josef Breu of University of Bayreuth, Germany and Mr. Felix Greuter of ABB, Switzerland for their valuable advices and suggestions and also to the *Elitenetzwerk*, *Bayern* for their financial support to carry out the research work.

References

[1] M. Matsuoka, Nonohmic properties of zinc oxide ceramics, Jpn. J. Appl. Phys. 10 (1971) 736–746.
[2] J.P. Guha, S. Kunej, D. Suvorov, Phase equilibrium relations in the binary system Bi_2O_3-ZnO, J. Mater. Sci. 39 (2004) 911–918.
[3] D.R. Clarke, Varistor ceramics, J. Am. Ceram. Soc. 82 (1999) 485–502, Nr. 3.
[4] J. Wong, Microstructure and phase transformation in a highly non-ohmic metal oxide varistor ceramic, J. Appl. Phys. 46 (4) (1975) 1653–1659.
[5] M. Inada, Crystal phases of nonohmic zinc oxide ceramics, Jpn. J. Appl. Phys. 17 (1) (1978) 1–10.
[6] M. Inada, Formation mechanism of nonohmic zinc oxide ceramics, Jpn. J. Appl. Phys. 19 (3) (1980) 409–419.
[7] G.C. Miles, A.R. West, Pyrochlore phases in the system ZnO–Bi_2O_3-Sb_2O_5: II. Crystal structures of $Zn_2Bi_{3.08}Sb_{2.92}O_{14+\delta}$ and $Zn_{2+x}Bi_{2.96-(x-y)}Sb_{3.04-y}O_{14.04+\delta}$, Solid State Sci. 8 (12) (2006) 1422–1429.
[8] J. Kim, T. Kimura, T. Yamaguchi, Sintering of zinc oxide doped with antimony oxide and bismuth oxide, J. Am. Ceram. Soc. 72 (1989) 1390–1395.
[9] K.G.V. Kumari, P.D. Vasu, V. Kumar, T. Asokan, P.K. Davies, Formation of zinc–antimony-based spinel phases, J. Am. Ceram. Soc. 85 (2001) 703–705.
[10] E.R. Leite, M.A.L. Nobre, E. Longo, J.A. Varela, Microstructural development of ZnO varistor during reactive liquid phase sintering, J. Mater. Sci. 31 (1996) 5391–5398.
[11] C.W. Bale, P. Chartrand, S.A. Degterov, G. Eriksson, K. Hack, R. Ben Mahfoud, J. Melancon, A.D. Pelton, S. Petersen, FactSage thermochemical software and databases, CALPHAD 26 (2002) 189–228.
[12] T. Takemura, M. Kobayashi, Y. Takada, K. Sato, High temperature X-ray diffraction measurements of ZnO varistor ceramics, Jpn. J. Appl. Phys. 25 (2) (1986) 295–296.
[13] J.H. Hubell, S.M. Seltzer, Tables of X-Ray Mass Attenuation Coefficients and Mass Energy-Absorption Coefficients, National Institute of Standards and Technology, Gaithersburg, Maryland, http://physics.nist.gov/PhysRefData/XrayMassCoef.
[14] D. Risold, B. Hallstedt, L.J. Gauckler, H.L. Lukas, S.G. Fries, The Bi–O system, J. Phase Equilib. 16 (1995) 223–234.
[15] C. de Capitani, T.H. Brown, The computation of chemical equilibrium in complex systems containing non-ideal solutions, Geochim. Cosmochim. Acta 51 (1987) 2639–2652.
[16] N.A. Asryan, A.S. Alikhanyan, G.D. Nipan, Thermodynamic stability of antimony oxides, J. Phys. Chem. 78 (1) (2004) 5–11.
[17] J. Kim, T. Kimura, T. Yamaguchi, Sintering of Sb_2O_3-doped ZnO, J. Mater. Sci. 24 (1989) 213–219.
[18] M. Trontelj, V. Kraševec, Effects of antimony oxide in the sintering of ZnO varistors, in: L.M. Levinson (Ed.), Advances in Varistor Technology, J. Am. Ceram. Soc., vol. 3, pp. 108–116.
[19] G. Werner, B. Freiberg, T. Reetz, V. Hilarius, Particle growth in ZnO powder, in: Proceedings of the 3rd International Conference of the European Ceramics Society, Madrid, Spain, (1993), pp. 827–832.